AIP | Applied Physics Letters

Beam tracking approach for single–shot retrieval of absorption, refraction, and dark–field signals with laboratory x–ray sources

Fabio A. Vittoria, Gibril K. N. Kallon, Dario Basta, Paul C. Diemoz, Ian K. Robinson, Alessandro Olivo, and Marco Endrizzi

Citation: Applied Physics Letters **106**, 224102 (2015); doi: 10.1063/1.4922189
View online: http://dx.doi.org/10.1063/1.4922189
View Table of Contents: http://scitation.aip.org/content/aip/journal/apl/106/22?ver=pdfcov
Published by the AIP Publishing

Beam tracking approach for single–shot retrieval of absorption, refraction, and dark–field signals with laboratory x–ray sources

Fabio A. Vittoria,[1,2,a)] Gibril K. N. Kallon,[1] Dario Basta,[1] Paul C. Diemoz,[1,2] Ian K. Robinson,[2,3] Alessandro Olivo,[1,2] and Marco Endrizzi[1]
[1]*Department of Medical Physics and Biomedical Engineering, University College London, Malet Place, Gower Street, London WC1E 6BT, United Kingdom*
[2]*Research Complex at Harwell, Harwell Oxford Campus, OX11 0FA Didcot, United Kingdom*
[3]*London Centre for Nanotechnology, WC1H 0AH London, United Kingdom*

(Received 30 March 2015; accepted 23 May 2015; published online 2 June 2015)

We present the translation of the beam tracking approach for x–ray phase–contrast and dark–field imaging, recently demonstrated using synchrotron radiation, to a laboratory setup. A single absorbing mask is used before the sample, and a local Gaussian interpolation of the beam at the detector is used to extract absorption, refraction, and dark–field signals from a single exposure of the sample. Multiple exposures can be acquired when high resolution is needed, as shown here. A theoretical analysis of the effect of polychromaticity on the retrieved signals, and of the artifacts this might cause when existing retrieval methods are used, is also discussed. [http://dx.doi.org/10.1063/1.4922189]

Over recent years, x-ray phase contrast imaging (XPCi) was proven to offer an excellent alternative to conventional absorption imaging when low density variations inside specimens have to be detected.[1,2] In fact, the additional sensitivity to phase results in improved image contrast, especially for weakly absorbing materials. Alongside XPCi, dark-field (or ultra–small–angle x–ray scatter[3]) imaging, which is sensitive to sample inhomogeneity on the sub–pixel scale, was proven to yield additional information in biomedical[4] and other applications.[5] The most commonly used XPCi techniques are: propagation–based,[6,7] analyzer–based,[8,9] grating interferometry,[10–12] and edge illumination.[13,14] In propagation–based XPCi no optical element is required. The recorded phase signal, however, is strongly affected by source size and detector resolution, which usually restrict its application to synchrotron facilities or microfocal sources. In analyzer–based methods, two crystals are used to create a narrow angular acceptance window for x–rays. This results in a very high sensitivity to small refraction angles but also makes the method impractical for implementation with polychromatic laboratory sources. Grating interferometry and edge illumination are the main techniques used for laboratory–based XPCi. They use two or three optical elements to generate and analyse a periodic intensity pattern on the detector. By acquiring a minimum of three images, while varying the relative displacement of the optical elements, it is possible to retrieve the absorption, refraction and scatter signals.[15,16] The presence of optical elements, however, plus the need for multiple acquisitions, leaves room for improvement in term of acquisition time, delivered dose, and stability requirements.

Recently, alternative "single-shot" XPCi methods have been proposed,[17–20] in which a reference pattern is created using either a sheet of sandpaper or the Talbot self–image from a phase grating, and correlation methods are used to analyse the local pattern distortions caused by a sample. While most of these were implemented at synchrotrons, Zanette *et al.*[20] extracted absorption, refraction, and dark–field signals from a speckle pattern using a laboratory setup. However, a speckle pattern will, in general, have a wide range of features with different size and intensity, resulting in a change of resolution and sensitivity across the image which could be difficult to control. This is not the case if the Talbot self–image of a grating is used; however, gratings employed at x-ray wavelengths typically have pitches of few micron, and a very high resolution detector is needed to resolve the intensity pattern. Moreover, the distance from the grating at which the self–image is created is energy dependent, resulting in a reduced pattern visibility when polychromatic sources are used.

We address these problems through a beam–tracking approach employing a single absorbing mask. This can be seen as the translation to a laboratory setup of the method we recently demonstrated with synchrotron radiation.[21] A scheme of the experimental setup is shown in Fig. 1: the

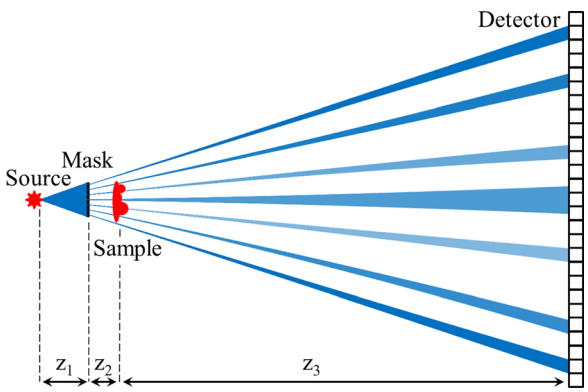

FIG. 1. Schematic diagram of the experimental setup.

[a)]Author to whom correspondence should be addressed. Electronic mail: fabio.vittoria.12@ucl.ac.uk

mask is used to create a series of physically separated beamlets that pass through the sample and reach the detector. Each beam is then analysed using a group of pixels, and absorption, refraction, and scattering are extracted from a single exposure. A similar setup has been proposed in the past[22,23] using different phase retrieval methods. In the method proposed by Krejci *et al.*,[22] two pixels per beam are illuminated (four in the 2D case), and analytical formulae are derived to calculate absorption and refraction. These, however, are based on a simplified description of the experimental setup that does not take into account important parameters such as source size, transmission through the mask, and pixel point spread function. In the method proposed by Wen *et al.*,[23] the above signals plus dark–field are retrieved by performing a Fourier–analysis of the intensity pattern. As will be shown later, however, when implemented with polychromatic radiation, this approach can lead to a mixing of absorption and scattering signals.

To demonstrate our approach, we used our "microscopy" setup,[24] based on a microfocus transmission tungsten target x–ray tube, operating at 80 kVp with source size of about 3.5 μm. The involved distances are: source to mask $z_1 = 13.2$ cm, mask to sample $z_2 = 2.1$ cm, and sample to detector $z_3 = 116.7$ cm. The mask is made of a 200 μm thick gold layer on a silicon substrate, with aperture size and period of 3 μm and 20 μm, respectively. The detector is a passive pixel CMOS sensor (Hamamatsu Photonics C9732DK), with pixel size of 50 μm. The geometrical magnification between the mask and the detector is $M = (z_1 + z_2 + z_3)/z_1 = 10$. The period of the intensity pattern at the detector plane is thus 200 μm, equal to four pixels. The system is aligned so that each beamlet hits the center of a pixel by using compact piezoelectric motors, and five pixels are used to track the variations of each beam.

Let us consider monochromatic radiation of energy E. An ideal absorbing mask can be described by the following complex transmission function:

$$G(x,E) = \sum_n rect[(x - nP)/W], \tag{1}$$

where P is the period of the mask, W is the dimension of the mask aperture, and $rect(x)$ is equal to 1 for $|x| < 1/2$ and 0 elsewhere. When a real mask is used, however, part of the beam can be transmitted through the absorbing septa. Referring for simplicity to one aperture only, the intensity transmitted through a real mask can be expressed as

$$|G(x,E)|^2 = [1 - o(E)]rect[x/W] + o(E), \tag{2}$$

where $o(E) = \exp[-2k\beta_m(E)T_m]$, with $\beta_m(E)$ being the imaginary part of the mask refractive index, T_m being the mask thickness, and $k = 2\pi/\lambda$, with λ being the x-ray wavelength. In the geometrical optics approximation, which is sufficiently accurate for our experimental setup,[25] the intensity recorded by each pixel can be expressed as

$$i(x,E) = p'(E)i_f(x,E) + p''(E), \tag{3}$$

where $p'(E) = p(E)[1 - o(E)]$, $p''(E) = p(E)o(E)$, and $i_f(x,E) = rect[x/(MW)] * PSF(x,E)$. $p(E)$ describes the source spectral distribution combined with the detector response at energy E, and * indicates the convolution with respect to the x variable. $PSF(x, E)$ is the convolution between the source intensity distribution projected at the detector plane and the detector point spread function, normalized such that $\int PSF(x,E)dx = 1$. When a sample is introduced, the intensity distribution measured by the detector can be expressed as[21]

$$\begin{aligned} i'(x,E) &= t(E)[i(x - \Delta(E),E) * s(x,E)] \\ &= t(E)p'(E)i_f(x - \Delta(E),E) * s(x,E) + t(E)p''(E), \end{aligned} \tag{4}$$

where $t(E)$ is the transmission through the sample, $\Delta(E)$ is the shift of the beam caused by refraction, and $s(E)$ is the sample scattering function. $s(E)$ is assumed as a normalized Gaussian with standard deviation $\sigma_s(E)$. The intensities measured in the polychromatic case, with and without the sample, are then calculated by integrating Eqs. (3) and (4) over energy

$$\begin{aligned} I(x) &= \int p'(E)i_f(x,E)dE \\ &\quad + \int p''(E)dE = I_F(x) + C_F, \end{aligned} \tag{5}$$

$$\begin{aligned} I'(x) &= \int t(E)p'(E)i_f(x - \Delta(E),E) * s(x,E)dE \\ &\quad + \int t(E)p''(E)dE = I_D(x) + C_D. \end{aligned} \tag{6}$$

For the case when the sample is not present, let us consider the total intensity A_F, mean value μ_F, and variance σ_F^2 of I_F, defined as follow:

$$A_F = \int I_F(x)dx, \tag{7}$$

$$\mu_F = \frac{\int xI_F(x)dx}{\int I_F(x)dx}, \tag{8}$$

$$\sigma_F^2 = \frac{\int (x - \mu_F)^2 I_F(x)dx}{\int I_F(x)dx}, \tag{9}$$

with analogous definitions for total intensity A_D, mean value μ_D and variance σ_D^2 of I_D (sample present). The variations between these parameters can be used to retrieve the sample's transmission (T), refraction (R), and scattering (S) signals, given by the following expressions:

$$T = \frac{A_D}{A_F} = \frac{\int p'(E)t(E)dE}{\int p'(E)dE}, \tag{10}$$

$$R = \mu_D - \mu_F = \frac{\int p'(E)t(E)\Delta(E)dE}{\int p'(E)t(E)dE}, \tag{11}$$

$$\begin{aligned} S = \sigma_D^2 - \sigma_F^2 &= \frac{\int p'(E)t(E)\sigma_s^2(E)dE}{\int p'(E)t(E)dE} \\ &\quad + \frac{\int p'(E)t(E)\Delta^2(E)dE}{\int p'(E)t(E)dE} - \left[\frac{\int p'(E)t(E)\Delta(E)dE}{\int p'(E)t(E)dE}\right]^2 \\ &\quad + \frac{\int p'(E)t(E)\sigma_f^2(E)dE}{\int p'(E)t(E)dE} - \frac{\int p'(E)\sigma_f^2(E)dE}{\int p'(E)dE}, \end{aligned} \tag{12}$$

where $\sigma_f^2(E)$ is the variance of $i_f(x,E)$. T is the ratio between the total intensity of the beam with and without the sample and is effectively the weighted average of $t(E)$ over the spectrum $p'(E)$. R indicates the average shift of the beam induced by refraction and is equal to the weighted average of $\Delta(E)$ over the spectrum $p'(E)$ multiplied by $t(E)$, which can be seen as an "effective spectrum" in the presence of the sample. The expression for the scattering signal is more complex and consists of different terms. The first term in the first line of Eq. (12) is the weighted average of $\sigma_s^2(E)$ over the effective spectrum $p'(E)t(E)$ and represents the "pure" scattering term. The second line of Eq. (12) is the variance of $\Delta(E)$ over the effective spectrum $p'(E)t(E)$ and explains how the variation of the refraction angle with energy results in an overall broadening of the beam, which will be measured as a scattering signal. The third line of Eq. (12) is a residual error in the normalization by the flat field signal σ_F^2 and depends on the difference in the spectrum without $(p'(E))$ and with $(p'(E)t(E))$ the sample. For a non–absorbing sample, this term would be equal to 0.

Let us assume that I_F and I_D can be approximated by Gaussian functions,[16] that the system is aligned so that $\mu_F = 0$, and that A_F and σ_F are known from an independent measurement without the sample. With these hypotheses, it is possible to retrieve T, R, and S by interpolating the intensity distribution $I'(x)$ measured by the detector with a Gaussian function, representing $I_D(x)$, plus a constant term, representing C_D.

We used a series of glass spheres, the leg of a beetle, and a wood section as samples. The intrinsic resolution of the system is comparable to the aperture width of the mask[24,26] and is therefore smaller than the mask period (which represents the rate at which the signal is sampled in a single exposure). To illuminate all the samples and avoid aliasing, for each acquisition, a 16–step sub–pixel scan along the direction orthogonal to the aperture lines was performed. The steps were then averaged in groups of 4, to obtain a final image with equal sampling step in the two directions (5.8 μm), and to reduce the noise. While this means that more than one exposure was acquired, the sub–pixel scan can be avoided in those cases where a final resolution in the scanning direction equal to the mask period can be accepted. Twenty exposures of 10 s were acquired for each step. Two flat field images were acquired, one before and one after the sample acquisition, with 40 exposures of 10 s each. I_F was measured by scanning the sample mask over 20 μm (one mask period) with 12 steps of 10 s each. The detector dark current was estimated by averaging 10 exposures of 10 s without x–rays and then subtracted from all the acquired images. To avoid artifacts from mask imperfections, the

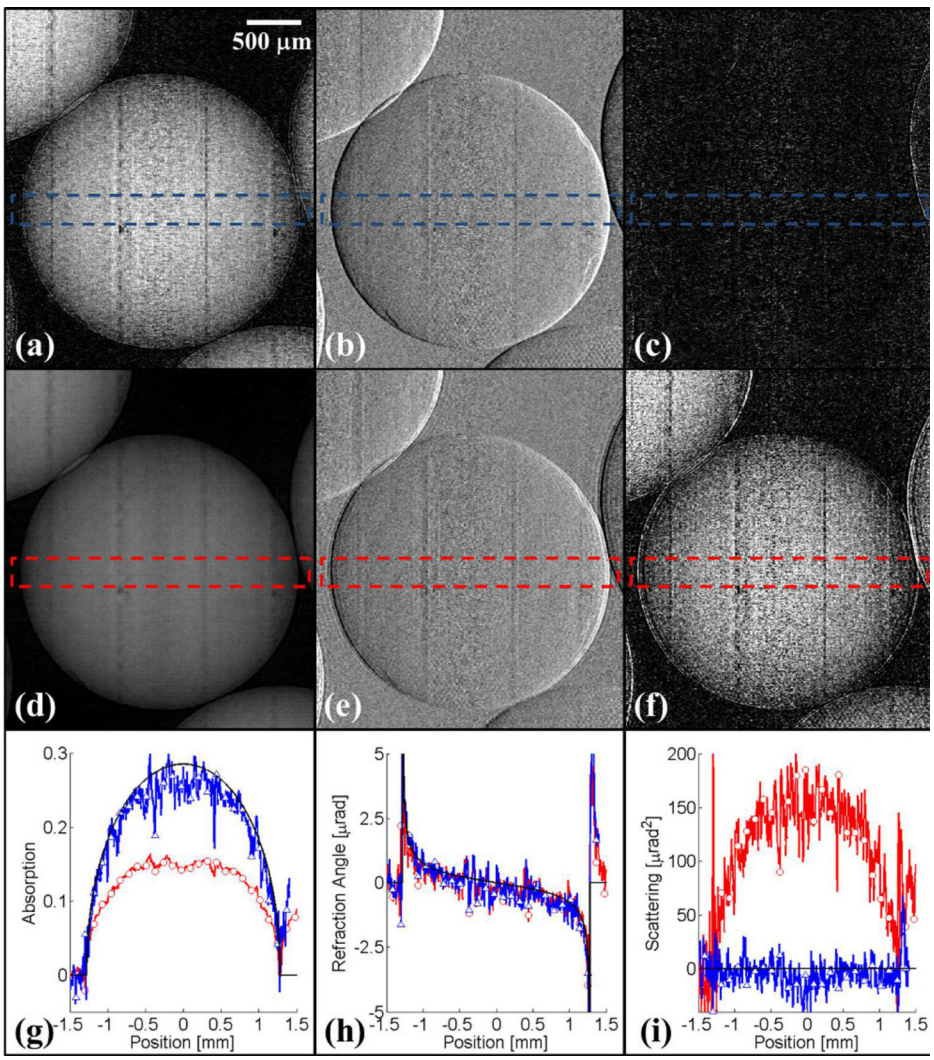

FIG. 2. Absorption $(-\log T)$ (a), refraction (R/z_3) (μrad) (b), and scattering (S/z_3^2) (μrad^2) (c) signals retrieved from glass spheres using the proposed method. (d), (e), and (f) show the same signals retrieved using Fourier–analysis.[23] In (g), (h), and (i), line profiles are extracted from the images (blue line and triangular marker for our method, red line and circular marker for Fourier–analysis), and compared with the expected value (black line). The vertical lines visible in the images are artifacts caused by mask imperfections.

images acquired with the sample were normalized by the flat field.

The result of the retrieval procedure applied to the spheres sample is shown in Figs. 2(a)–2(c). No scattering signal is visible, as expected for a homogeneous sample. We compared the proposed method with the "Fourier–analysis" one[23] (results shown in Figs. 2(d)–2(f)). A quantitative comparison between retrieved and theoretical signals is shown in Figs. 2(g)–2(i), with transmission and refraction calculated using Eqs. (10) and (11), and the theoretical scattering signal assumed to be 0. While our method yields good agreement, Fourier–analysis provides a signal lower than expected in absorption, and a relatively strong spurious scatter signal. This is an artifact caused by beam hardening. To explain it, let us consider Eqs. (5) and (6), in presence of absorption only. While the total intensity of the term $I_D(x)$ is reduced with respect to $I_F(x)$ by a factor T (see Eq. (10)), the term C_D is reduced by a factor of $T' = \int p''(E)t(E)dE / \int p''(E)dE$. The "Fourier–analysis" method, however, implicitly assumes that $I'(x) = TI(x)$ when only absorption is considered. While this is correct in the case of monochromatic radiation, it can cause artifacts in the polychromatic case, since the different absorption between the curve $I_D(x)$ and the offset C_D is retrieved as a scattering signal, i.e., the function $I'(x)$ appears to be broader than $I(x)$. In both methods, the presence of the offset has no direct influence on the retrieval of the refraction signal; hence the correct lateral shift between $I_D(x)$ and $I_F(x)$ is retrieved in both cases. To exclude that the described artifacts might originate in part also from other sources, the above results have also been validated through wave-optics simulations.[27]

Fig. 3 shows the results obtained from the beetle leg. No scattering signal is visible, and absorption is very weak; however, a strong refraction signal is detected, highlighting the importance of phase-contrast imaging for low absorbing materials. Finally, Fig. 4 shows the signals extracted from the wood sample, which we imaged because it is known to contain structures at different length scales. This results in features with dimensions smaller than the mask aperture

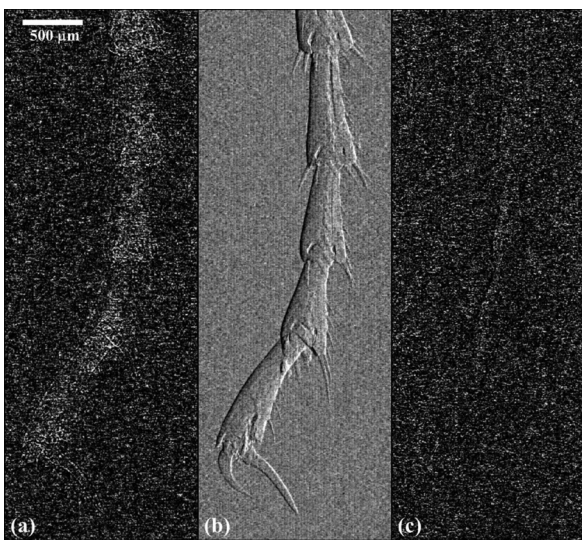

FIG. 3. Absorption $(-\log T)$ (a), refraction (R/z_3) (μrad) (b), and scattering (S/z_3^2) (μrad^2) (c) signals retrieved from the leg of a beetle.

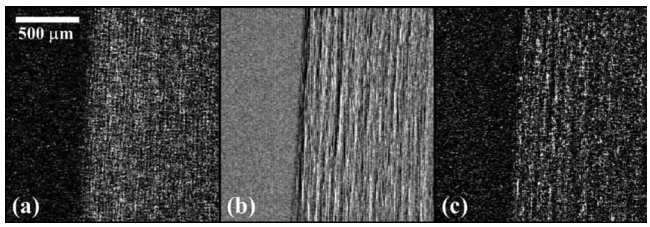

FIG. 4. Absorption $(-\log T)$ (a), refraction (R/z_3) (μrad) (b), and scattering (S/z_3^2) (μrad^2) (c) signals retrieved from a wood section.

producing the signal visible in the scatter image, while larger features produce a refraction signal.

In conclusion, we presented a method for the single–shot retrieval of absorption, refraction, and scattering in hard x-ray imaging, together with a detailed study of the effect of polychromaticity on the retrieved signals. The method has been tested both on a known object, obtaining a good agreement with the predicted values, and on more complex samples showing either weak or strong scattering. For this proof–of–concept experiment, a microfocal source was used with a high magnification, primarily to use a standard detector with 50 μm pixel size. However, the method can be easily extended to lower magnification values by using a detector with a smaller pixel size.

This work was funded by the EPSRC (Grant Nos. EP/I021884/1 and EP/I022562/1). P.C.D. and M.E. are supported by Marie Curie Career Integration Grants within the Seventh Framework Programme of the European Union, PCIG12-GA-2012-333990/334056.

[1]R. Fitzgerald, Phys. Today **53**(7), 23 (2000).
[2]S. W. Wilkins, Ya. I. Nesterets, T. E. Gureyev, S. C. Mayo, A. Pogany, and A. W. Stevenson, Philos. Trans. R. Soc. A **372**, 20130021 (2014).
[3]A. Bravin, P. Coan, and P. Suortti, Phys. Med. Biol. **58**, R1–R35 (2013).
[4]Z. Wang, N. Hauser, G. Singer, M. Trippel, R. A. Kubik–Huch, C. W. Schneider, and M. Stampanoni, Nat. Commun. **5**, 3797 (2014).
[5]C. Kottler, V. Revol, R. Kaufmann, C. Urban, N. Blanc, P. Niedermann, F. Cardot, and A. Dommann, AIP Conf. Proc. **1466**, 18 (2012).
[6]A. Snigirev, I. Snigireva, V. Kohn, S. Kuznetsov, and I. Schelokov, Rev. Sci. Instrum. **66**, 5486–5492 (1995).
[7]S. W. Wilkins, T. E. Gureyev, D. Gao, A. Pogany, and A. W. Stevenson, Nature **384**, 335–338 (1996).
[8]V. N. Ingal and E. A. Beliaevskaya, J. Phys. D: Appl. Phys. **28**, 2314–2317 (1995).
[9]D. Chapman, W. Thomlinson, R. E. Johnston, D. Washburn, E. Pisano, N. Gmur, Z. Zhong, R. Menk, F. Arfelli, and D. Sayers, Phys. Med. Biol. **42**, 2015–2025 (1997).
[10]C. David, B. Nohammer, H. H. Solak, and E. Ziegler, Appl. Phys. Lett. **81**, 3287–3289 (2002).
[11]A. Momose, S. Kawamoto, I. Koyama, Y. Hamaishi, K. Takai, and Y. Suzuki, Jpn. J. Appl. Phys., Part 2 **42**, L866–L868 (2003).
[12]F. Pfeiffer, T. Weitkamp, O. Bunk, and C. David, Nat. Phys. **2**, 258–261 (2006).
[13]A. Olivo, F. Arfelli, G. Cantatore, R. Longo, R. H. Menk, S. Pani, M. Prest, P. Poropat, L. Rigon, G. Tromba, E. Vallazza, and E. Castelli, Med. Phys. **28**, 1610–1619 (2001).
[14]A. Olivo and R. Speller, Appl. Phys. Lett. **91**, 074106 (2007).
[15]F. Pfeiffer, M. Bech, O. Bunk, P. Kraft, E. F. Eikenberry, C. Brönnimann, C. Grünzweig, and C. David, Nat. Mater. **7**, 134 (2008).
[16]M. Endrizzi, P. C. Diemoz, T. P. Millard, J. Louise Jones, R. D. Speller, I. K. Robinson, and A. Olivo, Appl. Phys. Lett. **104**, 024106 (2014).
[17]K. S. Morgan, D. M. Paganin, and K. K. W. Siu, App. Phys. Lett. **100**, 124102 (2012).
[18]S. Bérujon, E. Ziegler, R. Cerbino, and L. Peverini, Phys. Rev. Lett. **108**, 158102 (2012).

[19]K. S. Morgan, P. Modregger, S. C. Irvine, S. Rutishauser, V. A. Guzenko, M. Stampanoni, and C. David, Opt. Lett. **38**, 4605–4608 (2013).
[20]I. Zanette, T. Zhou, A. Burvall, U. Lundström, D. H. Larsson, M. Zdora, P. Thibault, F. Pfeiffer, and H. M. Hertz, Phys. Rev. Lett. **112**, 253903 (2014).
[21]F. A. Vittoria, M. Endrizzi, P. C. Diemoz, U. H. Wagner, C. Rau, I. K. Robinson, and A. Olivo, Appl. Phys. Lett. **104**, 134102 (2014).
[22]F. Krejci, J. Jakubek, and M. Kroupa, J. Instrum. **6**, C01073 (2011).
[23]H. H. Wen, E. E. Bennett, R. Kopace, A. F. Stein, and V. Pai, Opt. Lett. **35**, 1932–1934 (2010).
[24]M. Endrizzi, F. A. Vittoria, P. C. Diemoz, R. Lorenzo, R. D. Speller, U. H. Wagner, C. Rau, I. K. Robinson, and A. Olivo, Opt. Lett. **39**, 3332–3335 (2014).
[25]P. R. T. Munro, K. Ignatyev, R. D. Speller, and A. Olivo, Opt. Express **18**, 4103–4117 (2010).
[26]P. C. Diemoz, F. A. Vittoria, and A. Olivo, Opt. Express **22**, 15514–15529 (2014).
[27]See supplemental material at http://dx.doi.org/10.1063/1.4922189 for a validation of the obtained results through wave-optics simulations.